Originally published as:

Role of CO$_2$, climate and land use in regulating the seasonal amplitude increase of carbon fluxes in terrestrial ecosystems: a multimodel analysis

Fang Zhao[1,2], Ning Zeng[1,3], Ghassem Asrar[4], Pierre Friedlingstein[5], Akihiko Ito[7], Atul Jain[8], Eugenia Kalnay[1], Etsushi Kato[9], Charles D. Koven[10], Ben Poulter[11], Rashid Rafique[4], Stephen Sitch[6], Shijie Shu[8], Beni Stocker[12], Nicolas Viovy[13], Andy Wiltshire[14], and Sonke Zaehle[15]

[1]Department of Atmospheric and Oceanic Science, University of Maryland, College Park, MD 20742, USA
[2]Potsdam Institute for Climate Impact Research, Telegraphenberg, 14412 Potsdam, Germany
[3]Earth System Science Interdisciplinary Center, University of Maryland, College Park, MD 20742, USA
[4]Joint Global Change Research Institute, Pacific Northwest National Laboratory, College Park, MD 20742, USA
[5]University of Exeter, College of Engineering Mathematics and Physical Sciences, Exeter, EX4 4QF, UK
[6]University of Exeter, College of Life and Environmental Sciences, Exeter, EX4 4QF, UK
[7]Center for Global Environmental Research, National Institute for Environmental Studies, 305-0053 Tsukuba, Japan
[8]Department of Atmospheric Sciences, University of Illinois, Urbana, IL 61801, USA
[9]Global Environment Program Research & Development Division, the Institute of Applied Energy (IAE), 105-0003 Tokyo, Japan
[10]Earth Sciences Division, Lawrence Berkeley National Laboratory, Berkeley, CA 94720, USA
[11]Institute on Ecosystems and Department of Ecology, Montana State University, Bozeman, MT 59717, USA
[12]Climate and Environmental Physics, Physics Institute, University of Bern, 3012 Bern, Switzerland
[13]Laboratoire des Sciences du Climat et de l'Environnement, CEA CNRS UVSQ, 91191 Gif-sur-Yvette, France
[14]Hadley Centre, Met Office, Exeter, EX1 3PB, UK
[15]Biogeochemical Integration Department, Max Planck Institute for Biogeochemistry, P.O. Box 10 01 64, 07701 Jena, Germany

Correspondence to: Fang Zhao (fangzhao@pik-potsdam.de)

Abstract. We examined the net terrestrial carbon flux to the atmosphere (F_{TA}) simulated by nine models from the TRENDY dynamic global vegetation model project for its seasonal cycle and amplitude trend during 1961–2012. While some models exhibit similar phase and amplitude compared to atmospheric inversions, with spring drawdown and autumn rebound, others tend to rebound early in summer. The model ensemble mean underestimates the magnitude of the seasonal cycle by 40 % compared to atmospheric inversions. Global F_{TA} amplitude increase (19 ± 8 %) and its decadal variability from the model ensemble are generally consistent with constraints from surface atmosphere observations. However, models disagree on attribution of this long-term amplitude increase, with factorial experiments attributing 83 ± 56 %, -3 ± 74 and 20 ± 30 % to rising CO$_2$, climate change and land use/cover change, respectively. Seven out of the nine models suggest that CO$_2$ fertilization is the strongest control – with the notable exception of VEGAS, which attributes approximately equally to the three factors. Generally, all models display an enhanced seasonality over the boreal region in response to high-latitude warming, but a negative climate contribution from part of the Northern Hemisphere temperate region, and the net result is a divergence over climate change effect. Six of the nine models show that land use/cover change amplifies the seasonal cycle of global F_{TA}: some are due to forest regrowth, while others are caused by

crop expansion or agricultural intensification, as revealed by their divergent spatial patterns. We also discovered a moderate cross-model correlation between F_{TA} amplitude increase and increase in land carbon sink ($R^2 = 0.61$). Our results suggest that models can show similar results in some benchmarks with different underlying mechanisms; therefore, the spatial traits of CO_2 fertilization, climate change and land use/cover changes are crucial in determining the right mechanisms in seasonal carbon cycle change as well as mean sink change.

1 Introduction

The amplitude of the atmospheric CO_2 seasonal cycle is largely controlled by vegetation growth and decay in the Northern Hemisphere (NH) (Bacastow et al., 1985; Graven et al., 2013; Hall et al., 1975; Heimann et al., 1998; Pearman and Hyson, 1980; Randerson et al., 1997). Since 1958, atmospheric CO_2 measurements at Mauna Loa, Hawai'i, have tracked a 15 % rise in the peak-to-trough amplitude of the detrended CO_2 seasonal cycle (Zeng et al., 2014), suggesting an enhanced ecosystem activity due to changes in the strength of the ecosystem's production and respiration and to a shift in the timing of their phases (Randerson et al., 1997). In addition, some evidence suggests a latitudinal gradient in CO_2 amplitude increase in the NH, with a larger increase at Pt. Barrow, Alaska (0.6 % yr^{-1}) than at Mauna Loa (0.32 % yr^{-1}) (Graven et al., 2013; Randerson et al., 1999). Previous studies have attempted to attribute the long-term CO_2 amplitude increase to stimulated vegetation growth under rising CO_2 and increasing nitrogen deposition (Bacastow et al., 1985; Reich and Hobbie, 2013; Sillen and Dieleman, 2012). Another possible explanation offered is the effect of a warmer climate, especially in boreal and temperate regions, on the lengthening of growing season, enhanced plant growth (Keeling et al., 1996; Keenan et al., 2014), vegetation phenology (Thompson, 2011), ecosystem composition and structure (Graven et al., 2013). The agricultural green revolution, due to widespread irrigation, increasing management intensity and high-yield crop selection, could also contribute to the dynamics of the CO_2 seasonal amplitude (Zeng et al., 2014; Gray et al., 2014). Even though these studies are helpful in understanding the role of CO_2, climate and land use/cover changes, detailed knowledge of the relative contribution of these factors is still lacking.

Dynamic vegetation models are useful tools not only to disentangle effects of various mechanisms but also to offer insights on how terrestrial ecosystems respond to external changes. Attribution of the role of CO_2, climate and land use has been attempted with a single model (Zeng et al., 2014), but comprehensive multimodel assessment efforts are still missing. Two important questions must be addressed in such efforts, namely, whether the models can simulate observed CO_2 amplitude increase, and to what extent their factorial attributions agree. For the first question, the Coupled Model Intercomparison Project Phase 5 (CMIP5) Earth System Models seem to be able to simulate the amplitude increase measured at the Mauna Loa and Point Barrow surface stations (Zhao and Zeng, 2014); however, they underestimate the amplitude increase compared to upper air (3–6 km) observations significantly (Graven et al., 2013). It is possible that uncertainty in vertical mixing in atmospheric transport models (Yang et al., 2007), instead of biases in dynamic vegetation models themselves, causes the severe underestimation of upper air CO_2 amplitude increase. For the second question, in a unique modeling study conducted by McGuire et al. (2001), both CO_2 fertilization and land use/cover changes were found to contribute to CO_2 amplitude increase at Mauna Loa, but the four models disagreed on the role of climate and the relative importance of the factors they studied. Since then, no published study has explored the reliability of models' simulation of seasonal carbon cycle and quantified the relative contribution of various factors affecting it.

An important trait of the three main factors (i.e., CO_2, climate and land use/cover change) we consider in this study is their different regional influence. Rising CO_2 would likely enhance productivity in all ecosystems. Climate warming may affect high-latitude ecosystems more than tropical and subtropical vegetation, and droughts would severely affect plant growth in water-limited regions. Similarly, the effect of land use/cover change may be largely confined to agricultural fields and places with land conversion, mostly in midlatitude regions. Because of their different spatial traits, it is possible to determine which factor is most important with strategically placed observations. Forkel et al. (2016) recently derived a latitudinal gradient of CO_2 amplitude increase based on CO_2 observational data, which would provide strong support that high-latitude warming is the most important factor. However, with only two sites north of 60° N, the robustness of the result is limited. In lieu of additional observational evidence, as a first step, it is necessary to investigate how the models represent the regional patterns of seasonal change of carbon flux.

A number of recent studies have addressed different aspects of the seasonal amplitude topic. For example, the latitudinal gradient of CO_2 seasonal amplitude was used as benchmark in assessing the performance of JSBACH model (Dalmonech and Zaehle, 2013; Dalmonech et al., 2015). Based on a model intercomparison project – Multiscale Synthesis and Terrestrial Model Intercomparison Project (MsTMIP; Huntzinger et al., 2013; Wei et al., 2014) – Ito et al. (2016) focused on examining the relative contribution of CO_2, climate and land use/cover changes, but little model evaluation was performed. In order to further explore and understand the seasonal fluctuation of carbon fluxes, a more comprehensive study including both the model evaluation and factorial analysis is needed. The TRENDY model intercomparison project provides a nice platform for such analysis (Sitch et al., 2015).

Site-level model–data comparison of seasonal carbon fluxes has been performed extensively in Peng et al. (2015) for the first synthesis of TRENDY models. Using both the second synthesis of TRENDY models simulations and observations, in this study we aim to achieve two main goals. (1) Assess how well the models simulate the climatological seasonal cycle and seasonal amplitude change of the carbon flux against a number of observational-based datasets (CO$_2$ observations and atmospheric inversions). (2) Analyze the relative contribution from the three main factors (CO$_2$ fertilization, climate and land use/cover change) to the seasonal amplitude increase, both at the global and regional level.

2 Method

2.1 Terrestrial ecosystem models and TRENDY experiment design

Monthly net biosphere production (NBP) simulations for 1961–2012 from nine TRENDY models participating in the Global Carbon Project (Le Quéré et al., 2014) were examined (Table 1). A set of three offline experiments driven by either constant or varying climate data and other input such as atmospheric CO$_2$ and land use/cover forcing were designed in the TRENDY project to differentiate the role of CO$_2$, climate and land use (Table 2). We primarily evaluated results from the S3 experiment, where the models are driven by time-varying forcing data (Appendix A). In addition, we also used results from the S1 and S2 experiments.

2.2 Observations and observational-based estimates

In light of the large difference in the Coupled Climate Carbon Cycle Model Intercomparison Project (C^{4}MIP) models' sensitivity to CO$_2$ change (Friedlingstein et al., 2013), it is essential to evaluate whether the terrestrial biosphere models are able to capture important features of CO$_2$ seasonal cycle. The scarcity of observational constraints, especially the lack of long-term continuous observational records, limits our capacity to fully evaluate the dynamic processes in terrestrial ecosystem models. Nevertheless, in this study we make a first-order approximation of the evolution of the global CO$_2$ seasonal cycle, using limited CO$_2$ observation data. Following Zeng et al. (2014), monthly Mauna Loa records from 1961 to 2012 and a global monthly CO$_2$ index for the period of 1981–2012 were retrieved from NOAA's Earth System Research Laboratory (ESRL; www.esrl.noaa.gov/gmd/ccgg/trends/). Details on the data processing, choice of stations and quality control procedures in deriving the global CO$_2$ index (globally averaged CO$_2$ concentration) can be found in Thoning et al. (1989) and Masarie and Tans (1995).

Fluxes from process-based models can be directly compared with monthly gridded fluxes from atmospheric inversions, which combine measured atmospheric CO$_2$ concentration at multiple sites across the globe with atmospheric transport driven by meteorological data. Two representative inversions, Jena (Jena81 and Jena99, Rödenbeck et al., 2003) and the CarbonTracker (Peters et al., 2007), are included for comparison (Appendix B). For an exhaustive intercomparison of the atmospheric inversions, please refer to Peylin et al. (2013).

2.3 Calculating the seasonal cycle and its amplitude change

All monthly NBP- and inversion-derived fluxes are first re-sampled (box averaging, conserving mass) to a uniform $0.5° \times 0.5°$ global grid in units of $\mathrm{kg\,C\,m^{-2}\,yr^{-1}}$. For the TRENDY model simulations, we further define net carbon flux from the land to the atmosphere (F_{TA}), which simply reverses the sign of NBP, so that positive F_{TA} indicates net carbon release to the atmosphere, and negative F_{TA} indicates net carbon uptake. F_{TA} represents the sum of residual land sink and land use emission, including fluxes from ecosystem production and respiration, fire, harvest, etc.; although some models may not simulate all the processes. Changes in global atmospheric CO$_2$ concentration are then equal to F_{TA} plus ocean–atmosphere flux and fossil fuel emission. For inversion-derived fluxes, only terrestrial ecosystem fluxes are used (optimized global biosphere fluxes plus fire fluxes in CarbonTracker), which are conceptually similar to F_{TA}, except that atmospheric transport is included. Atmospheric transport can significantly affect local carbon fluxes (Randerson et al., 1997); however, the impact is limited on global and large zonal band totals.

The seasonal amplitudes of Mauna Loa Observatory CO$_2$ growth rate, global CO$_2$ growth rate and fluxes from model simulations and inversions are processed with a curve fitting package called CCGCRV from NOAA/ESRL (http://www.esrl.noaa.gov/gmd/ccgg/mbl/crvfit/crvfit.html). This package first filtered out the high-frequency signals with a series of internal steps involving polynomial and harmonic fitting, detrending and band-pass filtering, and then the amplitude is defined as the difference between each year's maximum and minimum. For the latitudinal plots only, we simply use maximum and minimum of each year to define the seasonal amplitude without first filtering the data. Previous studies (Graven et al., 2013; Randerson et al., 1997) have established that F_{TA} accounts for most of seasonal amplitude change from atmospheric CO$_2$, and the Mauna Loa CO$_2$ record is considered to represent the evolution of global mean CO$_2$ well (Kaminski et al., 1996). Therefore, similar to our earlier work (Zeng et al., 2014), we evaluated the amplitude change of modeled F_{TA} with Mauna Loa CO$_2$, ESRL's global CO$_2$ and the atmospheric inversions, to assess whether the models are able to capture both the global trend and latitudinal patterns. For relative amplitude changes, we compute the multimodel ensemble mean after deriving the time series (relative to their 1961–1970 mean) from individual model simulations, so that models with large amplitude change would not have a huge ef-

Table 1. Basic information for the nine TRENDY models used in this study.

Model name	Abbreviation	Spatial resolution	Nitrogen cycle	Fire simulation	Harvest flux	Reference
Community Land Model 4.5	CLM4.5BGC	$1.25° \times 0.94°$	yes	yes	no	Oleson et al. (2013)
ISAM	ISAM	$0.5° \times 0.5°$	yes	no	yes	Jain et al. (2013)
Joint UK Land Environment Simulator	JULES	$1.875° \times 1.25°$	no	no	no	Clark et al. (2011)
Lund-Potsdam-Jena	LPJ	$0.5° \times 0.5°$	no	yes	yes	Sitch et al. (2003)
LPX-Bern	LPX-Bern	$0.5° \times 0.5°$	yes	yes	yes	Stocker et al. (2014)
O-CN	OCN	$0.5° \times 0.5°$	yes	no	yes	Zaehle and Friend (2010)
ORCHIDEE	ORCHIDEE	$2° \times 2°$	no	no	yes	Krinner et al. (2005)
VEGAS	VEGAS	$0.5° \times 0.5°$	no	yes	yes	Zeng et al. (2005b)
VISIT	VISIT	$0.5° \times 0.5°$	no	yes	yes	Kato et al. (2013)

fect on the ensemble mean. Additionally, global and regional mean seasonal cycles over 2001–2010 between the models and inversions are compared. We further compared the seasonal amplitude of zonally averaged F_{TA} from TRENDY and atmospheric inversions. To smooth out minor variations but ensure similar phase in aggregation, we first resampled F_{TA} into 2.5° resolution, then summed it over latitude bands for the 2001–2010 mean F_{TA} seasonal cycle.

2.4 Factorial analyses

Relative amplitudes for 1961–2012 (relative to 1961–1970 mean seasonal amplitude) from the experiments S1, S2 and S3, respectively, are calculated using the CCGCRV package for each model, and a linear trend (in % yr^{-1}) is determined for that period. We use relative amplitude for percentage change to minimize impacts of some differing implementation choices like climate data in S1 (CO$_2$) among the models. The effect of CO$_2$ on the relative amplitude change is represented by a trend of S1 (CO$_2$ only) results; the S2 (CO$_2$ + climate) results show a trend that is the sum of CO$_2$ and climate effects, and the S3 (CO$_2$ + climate + land use/cover) simulations include trends from time-varying CO$_2$, climate and land use/cover change (abbreviated as land use for text and figures). For simplicity, the effect of "climate" as used in this paper includes the synergy of CO$_2$ and climate, and similarly the effect of "land use/cover" also includes the synergy terms. Therefore, the effects of CO$_2$, climate and land use/cover are then quantified as the trend for S1, the trend of S2 minus the S1 trend and the trend of S3 minus the S2 trend, respectively. Note that the synergy terms are likely small in some of the current generation dynamic vegetation models, such as those shown in previous sensitivity experiment results (Zeng et al., 2014).

2.5 Spatial attribution

Spatial attribution of global F_{TA} amplitude change can be difficult due to the phase difference at various latitudes. For example, the two amplitude peaks at northern and southern subtropics caused by monsoon movements are largely out of

phase, and the net contribution to global F_{TA} amplitude increase after their cancelation is small (Zeng et al., 2014). To quantify latitudinal and spatial contributions for each model, a unique quantity – $F_{k_A}^i$ – the difference between the maximum month (i_max) and the minimum month (i_min) of model i's global F_{TA}, based on model i's 2001–2010 mean seasonal cycle is defined as Eq. (1):

$$F_{k_A}^i = F_{k_{A(i\_\text{max})}}^i - F_{k_{A(i\_\text{min})}}^i. \tag{1}$$

The subscript k denotes the index of each latitudinal band or spatial grid, and A is the index of the year, ranging from 1961 to 2012. $F_{k_A}^i$ could be quite different for each model: for VEGAS, $F_{k_A}^i$ is F_{TA} in November (i_max = 11) minus F_{TA} in July (i_min = 7) in year A, and for LPJ, $F_{k_A}^i$ is F_{TA} in March (i_max = 3) minus F_{TA} in June (i_min = 6) in year A. The indexes i_max and i_min are fixed for each model, as summarized in Table 3. For all three experiments, $F_{k_A}^i$ is computed each year in 1961–2012 and at every latitude band or spatial grid (k), and then the trends of $F_{k_A}^i$ are calculated. The spatial aggregation of the resulted latitudinal-dependent trends would then approximately be equal to the trend of global F_{TA} maximum-minus-minimum seasonal amplitude.

3 Results

3.1 Mean seasonal cycle of F_{TA}

Four of the nine models (CLM4.5BGC, LPX-Bern, ORCHIDEE and VEGAS) simulate a mean global F_{TA} seasonal cycle of similar amplitude and phase compared with the Jena99 and CarbonTracker inversions (Fig. 1, Table 3). The other five models have much smaller seasonal amplitude than inversions, and the shape of the seasonal cycle is also notably different. As a result, the models' ensemble global F_{TA} has seasonal amplitude of 26.1 Pg C yr^{-1} during 2001–2010, about 40 % smaller than the inversions (Fig. 4 inset, Table 3). The model ensemble annual mean F_{TA} (residual land sink plus land use emission) is −1.1 Pg C yr^{-1} for 2001–2010, 30 % smaller than the inversions (Table 3). In some

models (ISAM, JULES and LPJ for the northern temperature region in Fig. 2) F_{TA} rebounds back quickly, resulting in a late summer F_{TA} maximum. The midsummer rebound is unlikely a model response to pronounced seasonal drought after 2000, as it is persistent in the mean seasonal cycle over every decade since 1961. A probable cause is the strong exponential response of soil respiration to temperature increase, which may lead to heterotopic respiration higher than net primary production (NPP) in summer. For example, HadGEM2-ES and HadCM3LC, which employ a forerunner of JULES3.2 used in this study, are found to have a comparatively better simulation of the seasonal cycle (Collins et al., 2011), due to a combination of a more sensitive temperature rate modifier combined with a larger seasonal soil temperature that is used in the later version of JULES. Alexandrov (2014) shows that both the amplitude underestimation and phase shift of F_{TA} seasonal cycle can be improved by increasing water use efficiency, decreasing temperature dependence of heterotrophic respiration and increasing the share of quickly decaying litterfall. Another probable factor is the simulation of plant phenology. With the help of remote sensing data, better phenology in model simulation has been shown to improve seasonal cycle simulation of carbon flux (Forkel et al., 2014). Additionally, the effect of carbon release from crop harvest is considered. If harvested carbon is the main cause for the midsummer rebound in some models, the rebound should be much less pronounced for the S2 (constant 1860 land use/cover) experiment, given that cropland area in 1860 is less than half of the 2000 level. However, based on the comparison between the S2 and S3 experiments over the global and northern temperate (major crop belts) F_{TA} seasonal cycle (Figs. S1 and S2 in the Supplement), the impact of harvested carbon flux is unlikely to explain the midsummer rebound. This is probably due to modeling efforts to prevent the sudden release of harvested carbon. Instead, carbon release of harvested products and/or their residuals is usually either spread over 12 months (i.e., LPJ, LPX-Bern, OCN, ORCHIDEE), or it enters soil litter carbon pool (i.e., ISAM) for subsequent decomposition over time.

TRENDY models and inversions agree best over the boreal region (Fig. 2a). While underestimating the global seasonal cycle, LPJ and VISIT both simulate similar boreal F_{TA} amplitude as inversions. In addition to ORCHIDEE and

VEGAS, LPJ and LPX-Bern also simulate maximum CO₂ drawdown in July for the boreal region, same as the inversions, while the other five models have the F_{TA} minimum in June. Large model spread is present for the northern temperate region, especially in summer. Both inversions and models agree marginally over the phase of the F_{TA} seasonal cycle in the tropics. The northern and southern tropics show seasonal cycles that are largely out of phase except for LPJ (Fig. 2c, d), due to the seasonal movement of the tropical rain belt in the intertropical convergence zone (ITCZ). The southern extratropics exhibit even smaller F_{TA} amplitude due to the relatively small biomass of the southern extratropics, and most
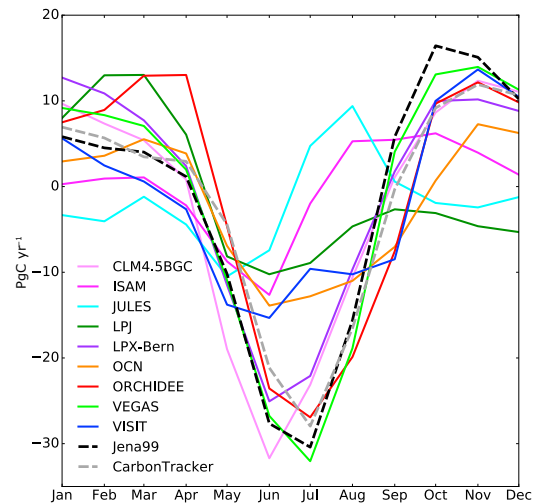

Figure 1. Mean seasonal cycle of global net carbon flux from nine TRENDY models (S3 experiment) and two inversions, Jena99 and CarbonTracker, averaged over 2001–2010.
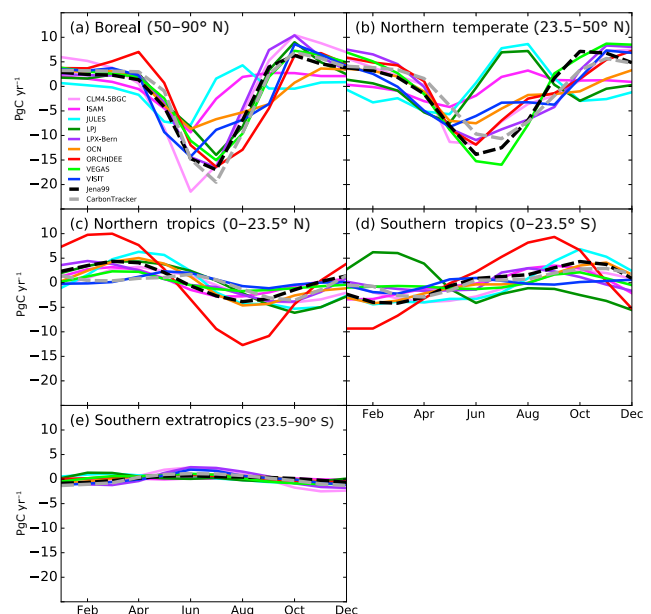

Figure 2. Mean seasonal cycle of net carbon flux totals over boreal (50–90° N), northern temperate (23.5–50° N), northern tropics (0–23.5° N), southern tropics (0–23.5° S) and southern extratropics (23.5–90° S) from nine TRENDY models and two inversions, Jena99 and CarbonTracker, averaged over 2001–2010.

models and inversions indicate a maximum F_{TA} around July, opposite in phase to its NH counterpart.

The latitudinal pattern of the multimodel median F_{TA} amplitude is remarkably similar to the inversions (Fig. 3). A notable feature is the large seasonality over the NH midlatitude to high-latitude region driven by temperature contrast between winter and summer. The model median also cap-

Table 2. Experimental design of TRENDY simulations.

Name	Time period	Atmospheric CO_2	Climate forcing	Land-use history**
S1	1901–2012	Time-varying	Constant*	Constant (1860)
S2			Time-varying	
S3				Time-varying

* Constant climate state is achieved by repeated or randomized or fixed climate cycles depending on each model.
** Only the crop, pasture and wood harvest information is included, so land use in this study refers specifically to the related agricultural and forestry processes.

Table 3. Global mean net land carbon flux, seasonal amplitude, the maximum and minimum months of F_{TA} for the nine TRENDY models and their ensemble mean during 1961–1970 and 2001–2010 periods. For the later period, characteristics of the atmosphere inversions Jena99 and CarbonTracker are also listed.

| Name	Net carbon flux		Seasonal amplitude		F_{TA}	F_{TA}
	$(Pg\,C\,yr^{-1})$		$(Pg\,C\,yr^{-1})$		minimum	maximum
	1961–1970	2001–2010	1961–1970	2001–2010	2001–2010	2001–2010
CLM4.5BGC	0.1	−2.4	38.4	44.3	Jun	Nov
ISAM	0.7	0.0	17.6	19.1	Jun	Oct
JULES	−0.2	−1.7	15.1	19.0	May	Aug
LPJ	1.3	−0.6	18.6	23.4	Jun	Mar
LPX-Bern	0.6	0.0	33.0	37.9	Jun	Jan
OCN	0.9	−1.8	16.1	21.6	Jun	Nov
ORCHIDEE	0.1	−0.7	35.7	39.9	Jul	Mar
VEGAS	−0.4	−1.5	40.7	46.7	Jul	Nov
VISIT	0.2	−1.4	25.3	28.9	Jun	Nov
Ensemble	0.4	−1.1	22.4	26.1	Jun	Nov
Jena99		−1.7		46.8	Jul	Oct
CarbonTracker		−1.6		39.9	Jul	Nov
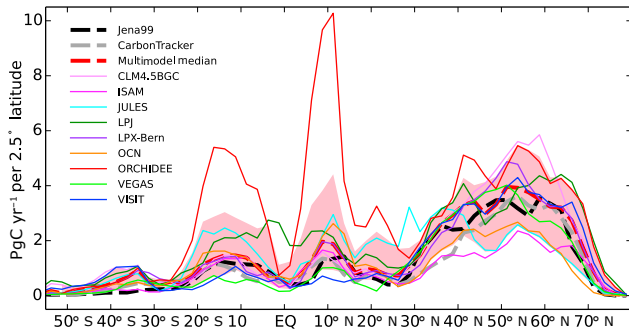
Figure 3. Latitudinal dependence of the seasonal amplitude of land–atmosphere carbon flux from the TRENDY multimodel median (red line, and the pink shading indicates the 10 to 90 percentile range of model spread), two atmospheric CO_2 inversions, Jena99 (black dashed line) and CarbonTracker (gray dashed line), and each individual model (thin line). Fluxes are first resampled to $2.5° \times 2.5°$, then summed over each $2.5°$ latitude band ($Pg\,C\,yr^{-1}$ per $2.5°$ latitude) for the TRENDY ensemble and inversions.

tures the two subtropical maxima around $10°$ N and $15°$ S that are caused by tropical monsoon movement. The main difference between the TRENDY models and the two inver-

sions is in the tropics and SH, where several models (JULES, LPJ, OCN and especially ORCHIDEE) show much higher amplitude than the inversions. Seasonal amplitude over 37–45 and 53–$60°$ N is also larger from TRENDY models than the inversions. A majority of the models display larger amplitude in the tropics and northern temperate regions. Only three models (ISAM, JULES and OCN) exhibit an underestimation of seasonal amplitudes north of $45°$ N. Because of phase difference among the models and at different latitudinal bands, for spatial and cross-model aggregated carbon fluxes, the seasonal amplitude is reduced. Similarly, analyses by Peng et al. (2015) with an earlier set of TRENDY models (Sitch et al., 2015) show an approximately equal number of models overestimating and underestimating carbon flux compared to flux sites north of $35°$ N. However, once the carbon fluxes of different phases are transported and mixed, seven out of nine models underestimate the CO_2 seasonal amplitude compared to CO_2 site measurements (Peng et al., 2015). Note that even at the same latitude band, factors like monsoons, droughts and spring snowmelt, etc. could lead to longitudinal difference in the phase of seasonal cycle (Figs. S3 and S4).
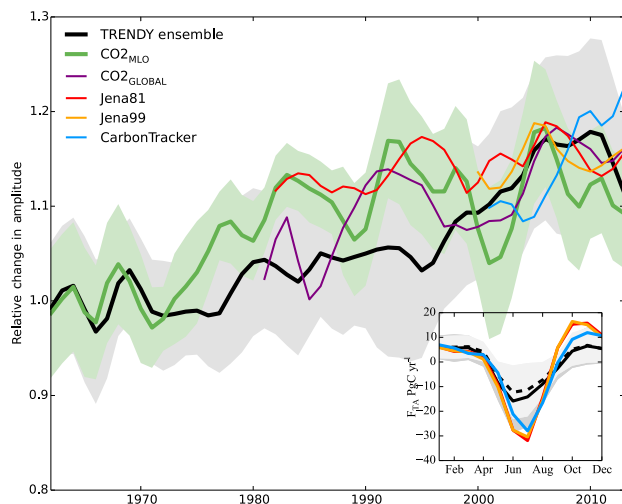
Figure 4. Trends for seasonal amplitude of TRENDY simulated multimodel ensemble mean land–atmosphere carbon flux F_{TA} (black), of the Mauna Loa Observatory (MLO) CO$_2$ mixing ratio (CO2$_{MLO}$, green) and global CO$_2$ mixing ratio (CO2$_{GLOBAL}$, purple), and of F_{TA} from atmospheric inversions of Jena81 (red), Jena99 (orange) and CarbonTracker (blue). The trends are relative to the 1961–1970 mean for the TRENDY ensemble and Mauna Loa CO$_2$, and the other time series are offset to have the same mean as the TRENDY ensemble for the last 10 years (2003–2012). A 9-year Gaussian smoothing (Harris, 1978) removes interannual variability for all time series, and its 1σ standard deviation is shown for CO2$_{MLO}$ (green shading). Note that the gray shading here instead indicates 1σ models' spread, which is generally larger than the standard deviation of the TRENDY ensemble's decadal variability. Inset: average seasonal cycles of models' ensemble mean F_{TA} (Pg C yr^{-1}) for the two periods: 1961–1970 (dashed line; lighter gray shading indicates 1σ model spread) and 2001–2010 (solid; darker gray shading indicates 1σ model spread), revealing enhanced CO$_2$ uptake during spring/summer growing season. Mean seasonal cycles global F_{TA} from the atmospheric inversions for 2001–2010 are also shown (same color as the main figure) for comparison.

3.2 Temporal evolution of F_{TA} seasonal amplitude

The seasonal amplitude of global total F_{TA} from the TRENDY model ensemble for 1961–2012 shows a long-term rise of 19 ± 8 %, with large decadal variability (Fig. 4). Similarly, the seasonal amplitude of CO$_2$ at Mauna Loa increases by 15 ± 3 % (0.85 ± 0.18 ppm) for the same period. This amplitude increase appears mostly as an earlier and deeper drawdown during the spring and summer growing season, mostly in June and July (Table 3, Fig. 4 inset). Changes in trend of yearly minima (indicating peak carbon uptake) and yearly maxima (dominated by respiration) contribute 91 ± 10 and 9 ± 10 % to the F_{TA} amplitude increase, respectively. Gurney and Eckels (2011) suggest trend in respiration increase is more important, but they averaged all months instead of using maxima and minima in their amplitude definition. The multimodel ensemble mean tracks some character-
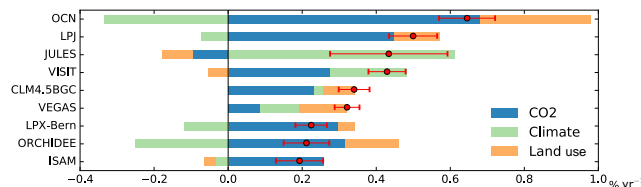

Figure 5. Attribution of the seasonal amplitude trend of global net land carbon flux for the period 1961–2012 to three key factors of CO$_2$, climate and land use/cover. The red dots represent models' global amplitude increase of F_{TA} from the S3 experiment, and error bars indicate 1σ standard deviation. The increasing seasonal amplitude of F_{TA} is decomposed into the influence of time-varying atmospheric CO$_2$ (blue), climate (light green) and land use/cover change (gold).

istics of the decadal variability reflected by the Mauna Loa record: stable in the 1960s, rise in the 1970–1980s, rapid rise in the early 2000s and decrease in the most recent 10 years. Strictly speaking, Mauna Loa CO$_2$ data are not directly comparable with simulated global F_{TA} because this single station is also influenced by atmospheric circulation as well as fossil fuel emissions and ocean–atmosphere fluxes. Nevertheless, the comparison of the long-term amplitude trend is still valuable because the Mauna Loa Observatory data constitute the only long-term record, and it is generally considered representative of global mean CO$_2$ (Heimann, 1986; Kaminski et al., 1996). The global total CO$_2$ index (CO2$_{GLOBAL}$) and F_{TA} from three atmospheric inversions are also included in the comparison. All data (Jena81, CO2$_{MLO}$, CO2$_{GLOBAL}$) show a decrease in seasonal amplitude in the late 1990s, possibly related to drought in the Northern Hemisphere midlatitude regions (Buermann et al., 2007; Zeng et al., 2005a), and about half of the models (LPJ, OCN, ORCHIDEE, VEGAS) also exhibit similar change (Fig. 7). Details on models' F_{TA} global and regional changes in 2001–2010 compared to 1961–1970 are listed in Table 4.

3.2.1 Attribution of global and regional F_{TA} seasonal amplitude

Models agree on increase of global F_{TA} seasonal amplitude during 1961–2012, but they disagree even in sign in the contribution of the different factors (Fig. 5). By computing the ratios between amplitude trends from rising CO$_2$, climate change and land use/cover change with the total trend for each model, we find that the effect of varying CO$_2$, climate and land use/cover contribute 83 ± 56, -3 ± 74 and 20 ± 30 % to the simulated global F_{TA} amplitude increase. All models simulate increasing amplitude for total F_{TA} in the boreal (50–90° N) and northern temperate (23.5–50° N) regions, and most models also indicate amplitude increase in the northern (0–23.5° N) and southern tropics (0–23.5° S) (Fig. 6). There is less agreement on the sign of amplitude change among the models in the southern extratropics (23.5–

Table 4. The seasonal amplitude (maximum minus minimum, in $Pg\,C\,yr^{-1}$) of mean net carbon flux for 2001–2010 relative to the 1961–1970 period, according to the nine TRENDY models (values are listed as percentage change in brackets, for both regions and the entire globe). The four large latitudinal regions are the same as in Fig. 3: boreal (50–90° N), temperate (23.5–50° N), northern tropics (0–23.5° N), southern tropics (0–23.5° S) and southern extratropics (23.5–90° S). Values from the two inversions, Jena99 and CarbonTracker, are also listed for comparison.

Name	Global	Boreal	Northern temperate	Northern tropics	Southern tropics	Southern extratropics
CLM4.5BGC	44.3 (15 %)	31.9 (17 %)	19.2 (15 %)	7.2 (22 %)	6.5 (−2 %)	4.9 (4 %)
ISAM	19.1 (9 %)	12.1 (11 %)	7.4 (13 %)	6.0 (1 %)	6.9 (−8 %)	0.4 (4 %)
JULES	19.0 (26 %)	12.2 (24 %)	14.3 (9 %)	11.6 (0 %)	11.3 (11 %)	2.2 (−24 %)
LPJ	23.4 (26 %)	23.0 (18 %)	14.7 (11 %)	10.5 (9 %)	11.8 (16 %)	2.0 (−12 %)
LPX-Bern	37.9 (15 %)	26.9 (10 %)	19.3 (6 %)	8.3 (9 %)	4.6 (−6 %)	4.2 (15 %)
OCN	21.6 (34 %)	12.3 (33 %)	11.1 (23 %)	9.7 (17 %)	8.3 (3 %)	2.0 (14 %)
ORCHIDEE	39.9 (12 %)	23.4 (14 %)	19.1 (5 %)	22.7 (9 %)	18.7 (2 %)	1.4 (37 %)
VEGAS	46.7 (15 %)	22.3 (17 %)	24.7 (10 %)	4.0 (11 %)	3.4 (12 %)	2.1 (6 %)
VISIT	28.9 (14 %)	22.9 (12 %)	15.6 (8 %)	3.4 (9 %)	3.2 (1 %)	3.1 (18 %)
Ensemble	26.1 (17 %)	18.0 (19 %)	12.4 (15 %)	8.0 (8 %)	4.9 (−3 %)	2.1 (13 %)
Jena99	46.8	23.3	21	8.2	8.5	1.5
CarbonTracker	39.9	26.5	16.3	5.3	5.8	2.4

90° S). Individual models' global and regional trends of F_{TA} amplitude attributable to the three factors (CO_2, climate and land use/cover) are listed in Table S1. For most models, latitudinal contribution to global F_{TA} amplitude (computed with $F_{k_A}^i$) shows that the pronounced midlatitude to high-latitude maxima in the NH dominate the simulated amplitude increase over 1961–2012 (Fig. 8, red dashed line for S3 results). All models also indicate a negative contribution from at least part of the northern temperate region.

The four models (CLM4.5BGC, VEGAS, LPX-Bern and ORCHIDEE) that simulate a more realistic mean global F_{TA} seasonal cycle (Fig. 1) are also relatively close in global F_{TA} seasonal amplitude, clustering around an increase of 14 ± 3 % during 1961–2012. Furthermore, they all suggest that land use/cover change contributes positively to global F_{TA} seasonal amplitude increase. On the other hand, four of the remaining five models (OCN, LPJ, JULES, VISIT) show a much larger rate of increase (26 ± 3 %), but given that these four models underestimate the mean amplitude by about 50 %, the absolute increase in global F_{TA} seasonal amplitude is actually similar (about $5\,Pg\,C\,yr^{-1}$) between the two groups of models. ISAM is an exception; it both underestimates the mean global F_{TA} seasonal amplitude and has the lowest rate of amplitude increase.

3.2.2 The rising CO_2 factor

Seven of the nine models suggest that the CO_2 fertilization effect is most responsible for the increase in the amplitude of global F_{TA}, while VEGAS attributes it to be approximately equal among the three factors (Fig. 5). The CO_2 fertilization effect alone seems to cause most of the amplitude increase in a majority of models, with notable contribution from climate

change and land use/cover change in CLM4.5BGC and VEGAS (Fig. 7). The effect of rising CO_2 appears to be slightly negative for JULES, possibly reflecting an offsetting of the strong seasonal soil respiration response found in this model. For each model, rising CO_2 in the boreal, northern temperate and the southern extratropics leads to a similar trend (Fig. 6). The magnitude of this trend may indicate each model's differing strength for CO_2 fertilization. This is possibly due to similar phases of F_{TA} seasonal cycle within the three regions that are mainly driven by climatological temperature contrast. The positive amplitude trend in the carbon flux of the northern and southern tropics from CO_2 fertilization is similar, and they likely would cancel out each other because their seasonal cycles are largely out of phase. Latitudinal contribution analyses reveal that the trend in the northern midlatitudes to high-latitudes is the main contributor to global F_{TA} amplitude increase when considering CO_2 fertilization effect alone (Fig. 8, blue line).

3.2.3 The climate change factor

The effect of climate change on F_{TA} amplitude is mixed: five models (OCN, LPJ, LPX-Bern, ORCHIDEE and ISAM) suggest climate change acts to decrease the F_{TA} amplitude, and four models (JULES, VISIT, CLM4.5BGC and VEGAS) suggest it is an increasing effect (Fig. 5). The high-latitude greening effect is evident in six out of nine models (Fig. 6), contributing, on average, 29 % of boreal amplitude increase. The latitudinal contribution analyses (Fig. 8) also suggest that warming-induced high-latitude "greening" effect is present in all models, but this positive contribution only exhibits a wide range of influence in about half of the models (CLM4.5BGC, JULES, VEGAS and VISIT).
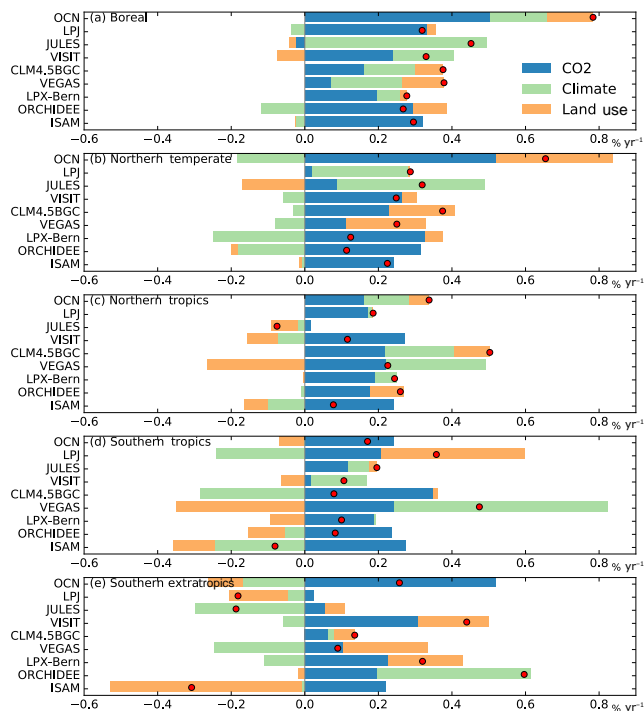
Figure 6. Attribution of the seasonal amplitude trend of regional (boreal (50–90° N), northern temperate (23.5–50° N), northern tropics (0–23.5° N), southern tropics (0–23.5° S) and southern extratropics (23.5–90° S)) net land carbon flux for the period 1961–2012 to three key factors CO$_2$, climate and land use/cover. The red dots represent models' global amplitude increase of F_{TA} from the S3 experiment. The increasing seasonal amplitude of F_{TA} is decomposed into the influence of time-varying atmospheric CO$_2$ (blue), climate (light green) and land use/cover change (gold).

The latitudinal patterns also reveal that, once climate change is considered, the contribution from the northern temperate region around 40° N shifts to negative in all models. In the northern temperate (23.5–50° N) region, climate change alone would decrease the F_{TA} amplitude – this is consistent among the four models with realistic mean global and northern temperate (Fig. 2) F_{TA} seasonal cycle simulation, but is not the case for JULES and LPJ (Fig. 6). Such decrease is possibly related to midlatitude drought (Buermann et al., 2007), which is consistent with findings by Schneising et al. (2014), who observed a negative relationship between temperature and seasonal amplitude of xCO_2 from both satellite measurements and CarbonTracker during 2003–2011 for the Northern temperate zone. The negative contribution from the temperate zone counteracts the positive boreal contribution, suggesting that the net impact from climate change on F_{TA} amplitude may not be as significant as previously suggested. With changing climate introduced, some models exhibit similar characteristics of decadal variability in global F_{TA} amplitude (Fig. 7). OCN and ORCHIDEE appear to be especially sensitive to the climate vari-
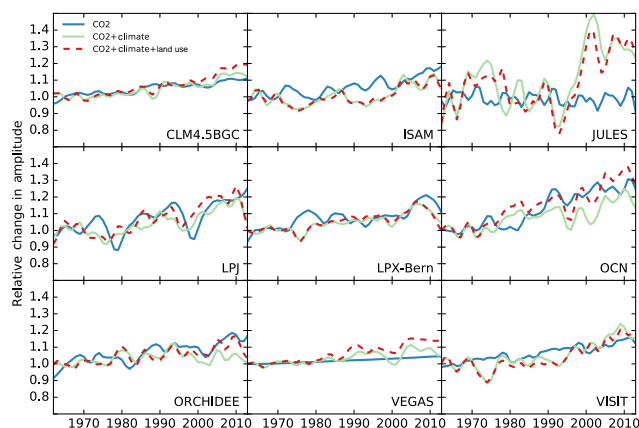

Figure 7. Trends for seasonal amplitude of global total net carbon fluxes from S1 (CO$_2$), S2 (CO$_2$+climate) and S3 (CO$_2$+climate+land use) for each individual TRENDY model. All amplitude time series are relative to their own 1961–1970 mean amplitude.

ations after the 1990s, resulting in a decrease in F_{TA} amplitude. It is also apparent from the time series figure that the strong increasing trend of F_{TA} amplitude from climate change in JULES is mostly due to the sharp rise from early 1990s to early 2000s, suggesting some possible model artifacts (Fig. 7). The effect of climate change is more mixed in both tropics and the southern extratropics.

3.2.4 The land use/cover change factor

Six of the nine models show that land use/cover change leads to increasing global F_{TA} amplitude (Fig. 5). Land use/cover change appears to amplify F_{TA} seasonal cycle in boreal and northern temperate regions for most models. For some models (VEGAS, CLM4.5BGC and OCN), this effect is especially pronounced in the northern temperate region where most of the global crop production takes place (Fig. 6). Note that the effect of land use/cover change includes two parts: one is the change of land use practice without changing the land cover type; the other is the change of land cover, including crop abandonment etc. VEGAS simulates the time-varying management intensity and the crop harvest index, which is an example of significant contribution from land use change (Zeng et al., 2014). For many other models, crops are treated as generic managed grasslands (i.e., CLM4.5BGC, LPJ), and land cover change is possibly the more important factor. During 1961–2012, large cropland areas were abandoned in the eastern United States and central Europe, and forest regrowth often followed. New cropland expanded in the tropics and South America, midwestern United States, eastern and central North Asia and the Middle East. How such changes affect the global F_{TA} amplitude is determined by the productivity and seasonal phase of the old and new vegetation covers. For CLM4.5BGC, JULES, LPJ and OR-

CHIDEE, enhanced vegetation activity from growing forest in these regions contributes positively to global F_{TA} amplitude increase (Fig. 9). In contrast, for LPX-Bern, VISIT and VEGAS in the eastern United States, a loss of cropland leads to a decrease in the amplitude. Additional cropland in the midwestern United States and eastern and central North Asia contributes negatively to the F_{TA} amplitude trend for JULES, LPJ and ORCHIDEE. These regions, however, are major zones contributing to the amplification of global F_{TA} for LPX-Bern, OCN, VEGAS and VISIT. One mechanism mentioned previously is agricultural intensification in VEGAS: in fact, CO$_2$ flux measurements over corn fields in the US Midwest show much larger seasonal amplitude than over nearby natural vegetation (Miles et al., 2012). Similarly, although croplands are treated as generic grassland, they still receive time-varying and spatially explicit fertilizer input in OCN (Zaehle et al., 2011). Another plausible mechanism is irrigation, which can alleviate adverse climate impact from droughts, and crops may have a stronger seasonal cycle than the natural vegetation they replace in these regions. The overall effect of land use/cover change for each model, therefore, is often the aggregated result over many regions that can only be revealed by spatially explicit patterns. When examining the latitudinal contribution only (Fig. 8), CLM4.5BGC, LPX-Bern, OCN and VEGAS are quite similar, even though the spatial patterns reveal that CLM4.5BGC is very different from the other three models (Fig. 9). For JULES, LPJ and ORCHIDEE a significant part of land use/cover change contribution comes from the tropical zone (Fig. 8). While most models indicate that land use/cover change in the southern tropics (Amazon is probably the most notable region) decreases global F_{TA} amplitude during 1961–2012, LPJ suggests that it would cause a large increase in the amplitude instead, possibly related to its different behavior in simulating the mean seasonal cycle of carbon flux for that region (Fig. 2d).

4 Discussion and conclusion

Our results show a robust increase of global and regional (especially over the boreal and northern temperate regions) F_{TA} amplitude simulated by all TRENDY models. During 1961–2012, TRENDY models' ensemble mean global F_{TA} relative amplitude increases (19 ± 8 %). Similarly, the CO$_2$ amplitude also increases (15 ± 3 %) at Mauna Loa for 1961–2012. This amplitude increase mostly reflects the earlier and deeper drawdown of CO$_2$ in the NH growing season. The models in general, especially the multimodel median, simulate latitudinal patterns of F_{TA} mean amplitude that are similar to the atmospheric inversions results. Their latitudinal patterns capture the temperature-driven seasonality from the NH mid-latitude to high-latitude region and the two monsoon-driven subtropical maxima, although the magnitude or extent vary. Despite the general agreements between the models' ensem-
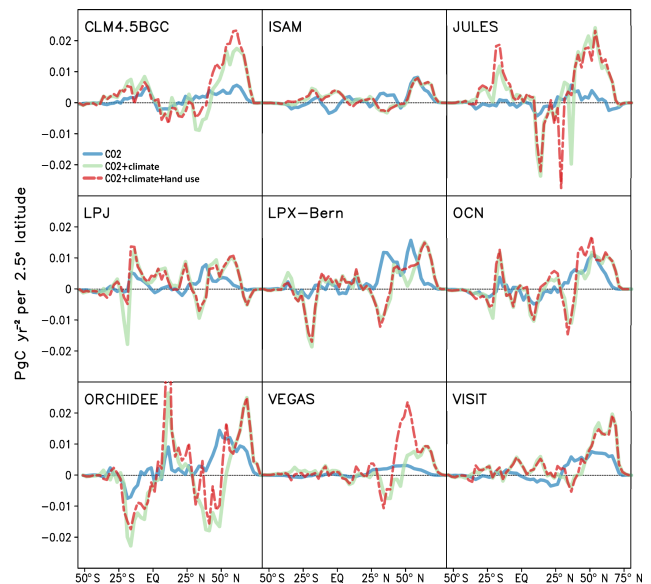

Figure 8. Latitudinal contribution of trends for seasonal amplitude of global land–atmosphere carbon flux from TRENDY models in the three sensitivity experiments. Fluxes are summed over each 2.5° latitude band (Pg C yr^{-1} per 2.5° latitude) before computing the $F_{k_A}^i$ (refer to the Methodology section for definition). For each 2.5° latitude band, the trend is calculated for the period 1961–2012.
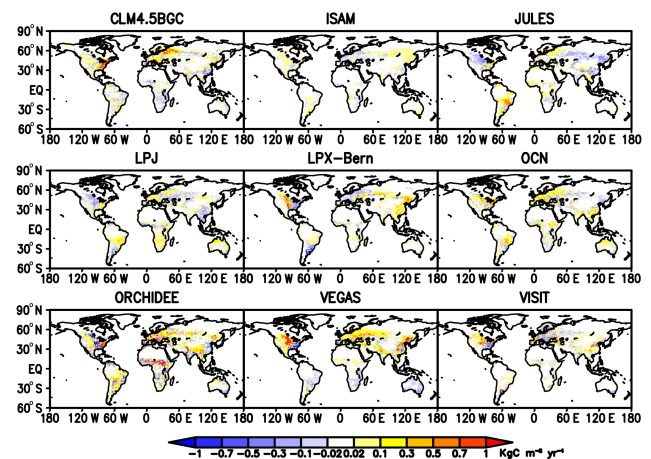

Figure 9. Contribution from land use/cover change on trends in the seasonal amplitude of global land–atmosphere carbon flux. For each spatial grid, the trend is computed as trends of the $F_{k_A}^i$ (refer to Methodology section for definition) in the S3 experiment (changing CO$_2$, climate and land use/cover) subtracted by trends in S2 (changing CO$_2$ and climate).

ble amplitude increases and the limited observation-based estimates, considerable model spread is noticeable. Five of the nine models considerably underestimate the global mean F_{TA} seasonal cycle compared to atmospheric inversions, and peak carbon uptake takes place 1 or 2 months too early in seven of the nine models. The seasonal amplitude of model ensem-

ble global mean F_{TA} is 40 % smaller than the amplitude of the atmosphere inversions. In contrast to the divergence in simulated seasonal carbon cycle, atmospheric inversions in Northern temperate and boreal regions are well constrained: 11 different inversions agree on July F_{TA} minimum in the Northern Hemisphere (25–90° N), with no more than 20 % difference in amplitude (Peylin et al., 2013).

The simulated amplitude increase is found to be mostly due to a larger F_{TA} minimum associated with a stronger ecosystem growth. Over the historical period, global mean carbon sink also increases over time, suggesting a possible relationship between seasonal amplitude and the mean sink (Ito et al., 2016; Randerson et al., 1997; Zhao and Zeng, 2014). The increasing trend of CO$_2$ amplitude, dominated by increasing trend of F_{TA} amplitude, has been interpreted as evidence for steadily increasing net land carbon sink (Keeling et al., 1995; Prentice et al., 2000). However, the increasing amplitude could also arise from (climatically induced) increased phase separation of photosynthesis and respiration, e.g., due to warming-induced earlier greening (Myneni et al., 1997). For the nine models, we found a moderate relationship between enhanced mean land carbon sink and the seasonal amplitude increase similar to reported results by in Zhao and Zeng (2014), with an R-squared value of 0.61 (Fig. 10). There might be some possibility in constraining change in land carbon sink with changes in observed CO$_2$ seasonal amplitude; however, extra caution should be given when interpreting this global-scale cross-model correlation, as there could be important regional differences that cancel out in aggregated global values. A factorial analysis of the long-term carbon uptake could help to determine which factor contributes to what extent to this correlation. Further research is also needed to explore the mechanisms behind such a relationship at continental scale, where more data from well-calibrated CO$_2$ monitoring sites and data on air–sea fluxes and atmospheric vertical transport could better constrain carbon balance (Prentice et al., 2001). Changes in residual land carbon sink estimates are also shown (Fig. 10), with the caveat that it is not directly comparable with simulated net carbon sink increase if there is a trend in simulated carbon flux changes associated with land cover conversion (deforestation, crop abandonment, etc.). Additionally, the decadal changes in residual and net land carbon sink are far from linear; instead, a sudden increase in mean land uptake occurred in 1988 (Beaulieu et al., 2012; Rafique et al., 2016; Sarmiento et al., 2010). With the aid of atmospheric transport, CO$_2$ amplitude trends at remote sites have benchmarking potential to constrain the models, especially with more observations and improved understanding of vegetation dynamics at regional level in the near future.

Models with a strong mean carbon sink (for example JULES and OCN) can have relatively weak seasonal amplitude, and the LPX-Bern model shows no carbon sink despite having a strong F_{TA} seasonality. Based on data from Table 8 of the Global Carbon Budget report (Le Quéré et al., 2014),
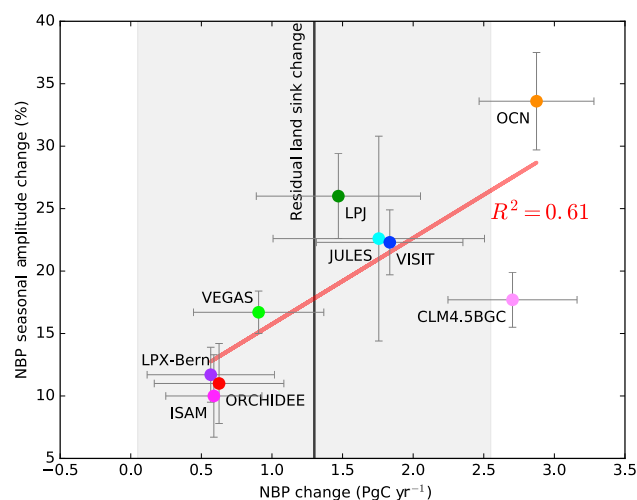

Figure 10. Relationship between the increase in net biosphere production (NBP, equal to $-F_{TA}$) and increase in NBP seasonal amplitude (as in Fig. 4's red dots), for the 1961–2012 period for nine TRENDY models. Error bars indicate the standard errors of the trend estimates. Increase in residual land sink is estimated by taking the difference between two residual land sinks, over 2004–2013 and 1960–1969 (an interval of 44 years), as reported in Le Quéré et al. (2015). This difference is then scaled by 52/44 (to make it comparable with models' NBP change for this figure), which is displayed by a black vertical line and shading (error added in quadrature, assuming Gaussian error for the two decadal residual land sinks, then also scaled). The cross-model correlation ($R^2 = 0.61$, $p < 0.05$) suggests that a model with a larger net carbon sink increase is likely to simulate a higher increase in NBP seasonal amplitude.

the net land carbon sink for 2000–2009 is estimated to be 1.5 ± 0.7 Pg C yr^{-1} (assuming Gaussian errors). Four models (JULES, OCN, VEGAS and VISIT) examined in this study are within the uncertainty range of this budget-based analysis. In spite of their similar mean land carbon sink, the shape of their F_{TA} seasonal cycle differs. While VEGAS also shows a similar seasonal carbon cycle compared to inversions, the other three models exhibit an unrealistically long carbon uptake period with half the amplitude as the inversions. July and August are the only 2 months with net carbon release for JULES, whereas OCN and VISIT both have a long major carbon uptake period from May to September. Given that the mean global and regional F_{TA} seasonal cycles are relatively well constrained in the northern extratropics, they can serve as a benchmark for terrestrial models (Heimann et al., 1998; Prentice et al., 2001). Insights gained from analyzing modeled seasonal amplitude of carbon flux may help to understand the considerable model spread found in the mean global carbon sink for the historical period (Le Quéré et al., 2015), which is possibly due to varied model sensitivity to different mechanisms (Arora et al., 2013). Examining details of different representations of important processes in models

could also help to better assess the different future projections on both the magnitude and direction of global carbon flux (Friedlingstein et al., 2006, 2013).

Unlike many previous studies that focused on comparing the season cycle at individual CO_2 monitoring stations (Peng et al., 2015; Randerson et al., 1997), we studied the global and large latitudinal bands. Such quantities often demonstrate well-constrained seasonality that is relatively robust against uncertainty from atmospheric transport, fossil fuel emission and biomass burning etc. We found greater uncertainty for the tropics and southern extratropics regions where atmospheric CO_2 observations are relatively sparse. Tropical ecosystems are also heavily affected by biomass burning; however, some models used in this study do not include fire dynamics. For models that simulate fire ignition/suppression, they are also varied by structure and complexity of fire-related processes, and many of them are prognostic (Poulter et al., 2015). It is not clear how fire would affect the F_{TA} seasonal cycle at global scale, and recent sensitivity study shows only minor differences among fire and "no fire" scenarios in CO_2 seasonal cycle at several observation stations (Poulter et al., 2015). These uncertainties, however, are unlikely to affect our main conclusions because of the limited contribution of tropics to global F_{TA} amplitude increase. Another possibly important factor is the impact from increased nitrogen deposition, which may have been included in the "CO_2 fertilization" effect for some models with full nitrogen cycle (Table 1); however, this can only be explored in future studies, as the TRENDY experiment design does not separate out the nitrogen contribution.

Our factorial analyses highlight fundamentally differential control from rising CO_2, climate change and land use/cover change among the models, with seven out of nine models indicating major contribution ($83 \pm 56\%$) to global F_{TA} amplitude increase from the CO_2 fertilization effect. The strength of CO_2 fertilization varies among models, but for each model, its magnitude in the boreal, northern temperate and southern extratropics regions is similar. Models are split regarding the role of climate change, as compared with the models' ensemble mean ($-3 \pm 74\%$). Regional analyses show that climate change amplifies the boreal F_{TA} seasonal cycle but weakens the seasonal cycle for other regions according to most models. By examining latitudinal trends from $F_{k_A}^i$, we found all models indicate a negative climate contribution over the midlatitudes, where droughts might have reduced ecosystem productivity. This negative effect offsets the high-latitude greening, which in some models results in a net negative climate change impact on global F_{TA} amplitude. Such a mechanism casts doubt on whether climate change is the main driver of the global F_{TA} amplitude increase. Land use/cover change, according to majority of the models, appears to amplify the global F_{TA} seasonal cycle ($20 \pm 30\%$); however, the mechanisms seem to differ among models. Conversion to/from cropland could either increase or decrease the seasonal amplitude, depending on how models

simulate the seasonal cycle of cropland compared to the natural vegetation it replaces/precedes. For the same pattern of increasing amplitude, the underlying causes could include irrigation mitigating negative climate effect, agricultural management practices and other mechanisms.

Overall, this study is largely helpful to enhance our understanding of the role of CO_2, climate change and land use/cover change in regulating the seasonal amplitude of carbon fluxes. In particular, models' disagreement in spatial pattern of carbon flux amplitude helps to identify optimal locations for additional CO_2 observations in the north. However, this work can be further improved through utilizing the CO_2 seasonal cycle and its amplitude at different locations as indicators to diagnose model behaviors. To achieve this, it is necessary to apply atmosphere transport on the simulated net carbon flux, along with ocean and fossil fuel fluxes, which would allow direct comparison with observed CO_2 amplitude change. In doing so, it is possible that models may overestimate CO_2 amplitude increase at most CO_2 observation stations if the simulated CO_2 fertilization effect is too strong.

5   Data availability

Appendix A: Environmental drivers for TRENDY

For observed rising atmospheric CO$_2$ concentration, the models use a single global annual (1860–2012) time series from ice cores (before 1958: Joos and Spahni, 2008) and the National Oceanic and Atmospheric Administration (NOAA)'s Earth System Research Laboratory (after 1958: monthly average from Mauna Loa and South Pole CO$_2$; South Pole data are constructed from the 1976–2014 average if not available). For climate forcing, the models employ 1901–2012 global climate data from the Climate Research Unit (CRU, version TS3.21, http://www.cru.uea.ac.uk; or CRU-National Centers for Environmental Prediction (NCEP) dataset, version 4, from N. Viovy (2011), unpublished data) at monthly (or interpolated to finer temporal resolution for individual models) temporal resolution and 0.5° × 0.5° spatial resolution. For land use/cover change history data, the models adopt either gridded yearly cropland and pasture fractional cover from the History Database of the Global Environment (HYDE) version 3.1 (http://themasites.pbl.nl/tridion/en/themasites/hyde/, (Klein Goldewijk et al., 2011), or the dataset including land use history transitions from L. Chini based on the HYDE data.

Appendix B: Atmospheric inversions

The Jena inversion is from the Max Planck Institute of Biogeochemistry, v3.7, at 5° × 5° spatial resolution (http://www.bgc-jena.mpg.de/christian.roedenbeck/download-CO2/, Rödenbeck et al., 2003), including two datasets abbreviated as Jena81 for the period of 1981–2010 using CO$_2$ data from 15 stations, and Jena99 using 61 stations for 1999–2010. Another inversion-based dataset used is the CarbonTracker, version CT2013B, from NOAA/ESRL at 1° × 1° spatial resolution (http://www.esrl.noaa.gov/gmd/ccgg/carbontracker/, Peters et al., 2007) for the period of 2000–2010, which integrates flask samples from 81 stations, 13 continuous measurement stations and 9 flux towers, and the surface fluxes from land and ocean carbon models as prior fluxes. These two inversion-based datasets are vastly different in their approach in inversion algorithm, choice of atmospheric data, transport model and prior information (Peylin et al., 2013). For example, to minimize the spurious variability introduced by changes in availability of observations, the Jena inversion provides multiple versions with different record length, each only using records covering its full period (for example, Jena99 includes more stations than Jena81, but with a shorter period). The CarbonTracker, however, opts for assimilating all quality-controlled data (with outliers removed), favoring a higher spatial resolution in estimated carbon fluxes. Therefore, we chose these two inversions to capture the uncertainty in atmospheric inversions to some extent.

The Supplement related to this article is available online at doi:10.5194/bg-13-5121-2016-supplement.

Edited by: A. V. Eliseev
Reviewed by: two anonymous referees

References

Alexandrov, G. A.: Explaining the seasonal cycle of the globally averaged CO_2 with a carbon-cycle model, Earth Syst. Dynam., 5, 345–354, doi:10.5194/esd-5-345-2014, 2014.

Arora, V. K., Boer, G. J., Friedlingstein, P., Eby, M., Jones, C. D., Christian, J. R., Bonan, G., Bopp, L., Brovkin, V., Cadule, P., Hajima, T., Ilyina, T., Lindsay, K., Tjiputra, J. F., and Wu, T.: Carbon–Concentration and Carbon–Climate Feedbacks in CMIP5 Earth System Models, J. Clim., 26, 5289–5314, doi:10.1175/JCLI-D-12-00494.1, 2013.

Bacastow, R. B., Keeling, C. D., and Whorf, T. P.: Seasonal amplitude increase in atmospheric CO_2 concetration at Mauna Loa, Hawaii, 1959–1982, J. Geophys. Res., 90, 10529–10540, doi:10.1029/JD090iD06p10529, 1985.

Beaulieu, C., Sarmiento, J. L., Mikaloff Fletcher, S. E., Chen, J., and Medvigy, D.: Identification and characterization of abrupt changes in the land uptake of carbon, Global Biogeochem. Cy., 26, 1–14, doi:10.1029/2010GB004024, 2012.

Buermann, W., Lintner, B. R., Koven, C. D., Angert, A., Pinzon, J. E., Tucker, C. J., and Fung, I. Y.: The changing carbon cycle at Mauna Loa Observatory, P. Natl. Acad. Sci. USA, 104, 4249–4254, 2007.

Clark, D. B., Mercado, L. M., Sitch, S., Jones, C. D., Gedney, N., Best, M. J., Pryor, M., Rooney, G. G., Essery, R. L. H., Blyth, E., Boucher, O., Harding, R. J., Huntingford, C., and Cox, P. M.: The Joint UK Land Environment Simulator (JULES), model description – Part 2: Carbon fluxes and vegetation dynamics, Geosci. Model Dev., 4, 701–722, doi:10.5194/gmd-4-701-2011, 2011.

Collins, W. J., Bellouin, N., Doutriaux-Boucher, M., Gedney, N., Halloran, P., Hinton, T., Hughes, J., Jones, C. D., Joshi, M., Liddicoat, S., Martin, G., O'Connor, F., Rae, J., Senior, C., Sitch, S., Totterdell, I., Wiltshire, A., and Woodward, S.: Development and evaluation of an Earth-System model – HadGEM2, Geosci. Model Dev., 4, 1051–1075, doi:10.5194/gmd-4-1051-2011, 2011.

Dalmonech, D. and Zaehle, S.: Towards a more objective evaluation of modelled land-carbon trends using atmospheric CO_2 and satellite-based vegetation activity observations, Biogeosciences, 10, 4189–4210, doi:10.5194/bg-10-4189-2013, 2013.

Dalmonech, D., Zaehle, S., Schürmann, G. J., Brovkin, V., Reick, C., and Schnur, R.: Separation of the Effects of Land and Climate Model Errors on Simulated Contemporary Land Carbon Cycle Trends in the MPI Earth System Model version 1*, J. Clim., 28, 272–291, doi:10.1175/JCLI-D-13-00593.1, 2015.

Forkel, M., Carvalhais, N., Schaphoff, S., v. Bloh, W., Migliavacca, M., Thurner, M., and Thonicke, K.: Identifying environmental controls on vegetation greenness phenology through model-data integration, Biogeosciences, 11, 7025–7050, doi:10.5194/bg-11-7025-2014, 2014.

Forkel, M., Carvalhais, N., Rödenbeck, C., Keeling, R., Heimann, M., Thonicke, K., Zaehle, S., and Reichstein, M.: Enhanced seasonal CO_2 exchange caused by amplified plant productivity in northern ecosystems, Science, 351, 696–699, doi:10.1126/science.aac4971, 2016.

Friedlingstein, P., Cox, P., Betts, R., Bopp, L., Von Bloh, W., Brovkin, V., Cadule, P., Doney, S., Eby, M., Fung, I., Bala, G., John, J., Jones, C., Joos, F., Kato, T., Kawamiya, M., Knorr, W., Lindsay, K., Matthews, H. D., Raddatz, T., Rayner, P., Reick, C., Roeckner, E., Schnitzler, K. G., Schnur, R., Strassmann, K., Weaver, A. J., Yoshikawa, C., and Zeng, N.: Climate-carbon cycle feedback analysis: Results from the (CMIP)-M-4 model intercomparison, J. Clim., 19, 3337–3353, doi:10.1175/jcli3800.1, 2006.

Friedlingstein, P., Meinshausen, M., Arora, V. K., Jones, C. D., Anav, A., Liddicoat, S. K., and Knutti, R.: Uncertainties in CMIP5 climate projections due to carbon cycle feedbacks, J. Clim., 27, 511–526, doi:10.1175/JCLI-D-12-00579.1, 2013.

Graven, H. D., Keeling, R. F., Piper, S. C., Patra, P. K., Stephens, B. B., Wofsy, S. C., Welp, L. R., Sweeney, C., Tans, P. P., Kelley, J. J., Daube, B. C., Kort, E. A., Santoni, G. W., and Bent, J. D.: Enhanced Seasonal Exchange of CO_2 by Northern Ecosystems Since 1960, Science, 341, 1085–1089, doi:10.1126/science.1239207, 2013.

Gray, J. M., Frolking, S., Kort, E. A., Ray, D. K., Kucharik, C. J., Ramankutty, N., and Friedl, M. A.: Direct human influence on atmospheric CO_2 seasonality from increased cropland productivity, Nature, 515, 398–401, doi:10.1038/nature13957, 2014.

Gurney, K. R. and Eckels, W. J.: Regional trends in terrestrial carbon exchange and their seasonal signatures, Tellus B, 63, 328–339, doi:10.1111/j.1600-0889.2011.00534.x, 2011.

Hall, C. A. S., Ekdahl, C. A., and Wartenberg, D. E.: A fifteen-year record of biotic metabolism in the Northern Hemisphere, Nature, 255, 136–138, doi:10.1038/255136a0, 1975.

Harris, F. J.: On the use of windows for harmonic analysis with the discrete Fourier transform, P. IEEE, 66, 51–83, doi:10.1109/PROC.1978.10837, 1978.

Heimann, M.: The Changing Carbon Cycle, a Global Analysis, edited by: Trabalka, J. R. and Reichle, D. E., Springer, New York, 1986.

Heimann, M., Esser, G., Haxeltine, A., Kaduk, J., Kicklighter, D. W., Knorr, W., Kohlmaier, G. H., Mcguire, A. D., Melillo, J., Moore, B., Ottofi, R. D., Prentice, I. C., Sauf, W., Schloss, A., Sitch, S., Wittenberg, U., and Wtirth, G.: Evaluation of terrestrial carbon cycle models through simulations of the seasonal cycle of atmospheric First results of a model intercomparison study, Global Biogeochem. Cy., 12, 1–24, 1998.

Huntzinger, D. N., Schwalm, C., Michalak, A. M., Schaefer, K., King, A. W., Wei, Y., Jacobson, A., Liu, S., Cook, R. B., Post, W. M., Berthier, G., Hayes, D., Huang, M., Ito, A., Lei, H., Lu, C., Mao, J., Peng, C. H., Peng, S., Poulter, B., Riccuito, D., Shi, X., Tian, H., Wang, W., Zeng, N., Zhao, F., and Zhu, Q.: The North American Carbon Program Multi-Scale Synthesis and Terrestrial Model Intercomparison Project – Part 1: Overview and experimental design, Geosci. Model Dev., 6, 2121–2133, doi:10.5194/gmd-6-2121-2013, 2013.

Ito, A., Inatomi, M., Huntzinger, D., Schwalm, C., Michalak, A., Cook, R., King, A., Mao, J., Wei, Y., Post, W. Mac, Wang, W., Arain, M. A., Huang, S., Hayes, D., Ricciuto, D., Shi, X., Huang, M., Lei, H., Tian, H., Lu, C., Yang, J., Tao, B., Jain, A., Poulter, B., Peng, S., Ciais, P., Fisher, J., Parazoo, N., Schaefer, K., Peng, C., Zeng, N., and Zhao, F.: Decadal trends in the seasonal-cycle amplitude of terrestrial CO₂ exchange resulting from the ensemble of terrestrial biosphere models, Tellus B, 68, 28968, doi:10.3402/tellusb.v68.28968, 2016.

Jain, A. K., Meiyappan, P., Song, Y., and House, J. I.: CO₂ emissions from land-use change affected more by nitrogen cycle, than by the choice of land-cover data, Glob. Change Biol., 19, 2893–906, doi:10.1111/gcb.12207, 2013.

Joos, F. and Spahni, R.: Rates of change in natural and anthropogenic radiative forcing over the past 20,000 years, P. Natl. Acad. Sci. USA, 105, 1425–1430, doi:10.1073/pnas.0707386105, 2008.

Kaminski, T., Giering, R., and Heimann, M.: Sensitivity of the seasonal cycle of CO₂ at remote monitoring stations with respect to seasonal surface exchange fluxes determined with the adjoint of an atmospheric transport model, Phys. Chem. Earth, 21, 457–462, 1996.

Kato, E., Kinoshita, T., Ito, A., Kawamiya, M., and Yamagata, Y.: Evaluation of spatially explicit emission scenario of land-use change and biomass burning using a process-based biogeochemical model, J. Land Use Sci., 8, 104–122, doi:10.1080/1747423X.2011.628705, 2013.

Keeling, C. D., Whorf, T. P., Wahlen, M., and van der Plichtt, J.: Interannual extremes in the rate of rise of atmospheric carbon dioxide since 1980, Nature, 375, 666–670, doi:10.1038/375666a0, 1995.

Keeling, C. D., Chin, J. F. S., and Whorf, T. P.: Increased activity of northern vegetation inferred from atmospheric CO₂ measurements, Nature, 382, 146–149, doi:10.1038/382146a0, 1996.

Keenan, T., Gray, J., and Friedl, M.: Net carbon uptake has increased through warming-induced changes in temperate forest phenology, Nature Climate Change, 4, 598–604, doi:10.1038/NCLIMATE2253, 2014.

Klein Goldewijk, K., Beusen, A., Van Drecht, G., and De Vos, M.: The HYDE 3.1 spatially explicit database of human-induced global land-use change over the past 12,000 years, Global Ecol. Biogeogr., 20, 73–86, doi:10.1111/j.1466-8238.2010.00587.x, 2011.

Krinner, G., Viovy, N., de Noblet-Ducoudré, N., Ogée, J., Polcher, J., Friedlingstein, P., Ciais, P., Sitch, S., and Prentice, I. C.: A dynamic global vegetation model for studies of the coupled atmosphere-biosphere system, Global Biogeochem. Cy., 19, GB1015, doi:10.1029/2003GB002199, 2005.

Le Quéré, C., Peters, G. P., Andres, R. J., Andrew, R. M., Boden, T. A., Ciais, P., Friedlingstein, P., Houghton, R. A., Marland, G., Moriarty, R., Sitch, S., Tans, P., Arneth, A., Arvanitis, A., Bakker, D. C. E., Bopp, L., Canadell, J. G., Chini, L. P., Doney, S. C., Harper, A., Harris, I., House, J. I., Jain, A. K., Jones, S. D., Kato, E., Keeling, R. F., Klein Goldewijk, K., Körtzinger, A., Koven, C., Lefèvre, N., Maignan, F., Omar, A., Ono, T., Park, G.-H., Pfeil, B., Poulter, B., Raupach, M. R., Regnier, P., Rödenbeck, C., Saito, S., Schwinger, J., Segschneider, J., Stocker, B. D., Takahashi, T., Tilbrook, B., van Heuven, S., Viovy, N., Wanninkhof, R., Wiltshire, A., and Zaehle, S.: Global carbon budget 2013, Earth Syst. Sci. Data, 6, 235–263, doi:10.5194/essd-6-235-2014, 2014.

Le Quéré, C., Moriarty, R., Andrew, R. M., Peters, G. P., Ciais, P., Friedlingstein, P., Jones, S. D., Sitch, S., Tans, P., Arneth, A., Boden, T. A., Bopp, L., Bozec, Y., Canadell, J. G., Chini, L. P., Chevallier, F., Cosca, C. E., Harris, I., Hoppema, M., Houghton, R. A., House, J. I., Jain, A. K., Johannessen, T., Kato, E., Keeling, R. F., Kitidis, V., Klein Goldewijk, K., Koven, C., Landa, C. S., Landschützer, P., Lenton, A., Lima, I. D., Marland, G., Mathis, J. T., Metzl, N., Nojiri, Y., Olsen, A., Ono, T., Peng, S., Peters, W., Pfeil, B., Poulter, B., Raupach, M. R., Regnier, P., Rödenbeck, C., Saito, S., Salisbury, J. E., Schuster, U., Schwinger, J., Séférian, R., Segschneider, J., Steinhoff, T., Stocker, B. D., Sutton, A. J., Takahashi, T., Tilbrook, B., van der Werf, G. R., Viovy, N., Wang, Y.-P., Wanninkhof, R., Wiltshire, A., and Zeng, N.: Global carbon budget 2014, Earth Syst. Sci. Data, 7, 47–85, doi:10.5194/essd-7-47-2015, 2015.

Masarie, K. A. and Tans, P. P.: Extension and integration of atmospheric carbon dioxide data into a globally consistent measurement record, J. Geophys. Res., 100, 11593, doi:10.1029/95JD00859, 1995.

McGuire, A. D., Sitch, S., Clein, J. S., Dargaville, R., Esser, G., Foley, J., Heimann, M., Joos, F., Kaplan, J., Kicklighter, D. W., Meier, R. A., Melillo, J. M., Moore III, B., Prentice, I. C., Ramankutty, N., Reichenau, T., Schloss, A., Tian, H., Williams, L. J., and Wittenberg, U.: Carbon balance of the terrestrial biosphere in the twentieth century: Analyses of CO₂, climate and land use effects with four process-based ecosystem models, Global Biogeochem. Cy., 15, 183–206, 2001.

Miles, N. L., Richardson, S. J., Davis, K. J., Lauvaux, T., Andrews, A. E., West, T. O., Bandaru, V., and Crosson, E. R.: Large amplitude spatial and temporal gradients in atmospheric boundary layer CO₂ mole fractions detected with a tower-based network in the U.S. upper Midwest, J. Geophys. Res.-Biogeo., 117, 1–13, doi:10.1029/2011JG001781, 2012.

Myneni, R. B., Keeling, C. D., Tucker, C. J., Asrar, G., and Nemani, R. R.: Increased plant growth in the northern high latitudes from 1981 to 1991, Nature, 386, 698–702, doi:10.1038/386698a0, 1997.

Oleson, K., Lawrence, D., Bonan, G., Drewniak, B., Huang, M., Koven, C., Levis, S., Li, F., Riley, W., Subin, Z., Swenson, S., Thornton, P., Bozbiyik, A., Fisher, R., Heald, C., Kluzek, E., Lamarque, J.-F., Lawrence, P., Leung, L., Lipscomb, W.,

Muszala, S., Ricciuto, D., Sacks, W., Sun, Y., Tang, J., and Yang, Z.-L.: Technical description of version 4.5 of the Community Land Model (CLM), available at: http://opensky.library.ucar.edu/collections/TECH-NOTE-000-000-000-870 (last access: 30 August 2015), 2013.

Pearman, G. I. and Hyson, P.: Activities of the Global Biosphere as Reflected in Atmospheric CO_2 Records, J. Geophys. Res., 85, 4457–4467, 1980.

Peng, S., Ciais, P., Chevallier, F., Peylin, P., Cadule, P., Sitch, S., Piao, S., Ahlström, A., Huntingford, C., Levy, P., Li, X., Liu, Y., Lomas, M., Poulter, B., Viovy, N., Wang, T., Wang, X., Zaehle, S., Zeng, N., Zhao, F., and Zhao, H.: Benchmarking the seasonal cycle of CO_2 fluxes simulated by terrestrial ecosystem models, Global Biogeochem. Cy., 29, 46–64, doi:10.1002/2014GB004931, 2015.

Peters, W., Jacobson, A. R., Sweeney, C., Andrews, A. E., Conway, T. J., Masarie, K., Miller, J. B., Bruhwiler, L. M. P., Pétron, G., Hirsch, A. I., Worthy, D. E. J., van der Werf, G. R., Randerson, J. T., Wennberg, P. O., Krol, M. C., and Tans, P. P.: An atmospheric perspective on North American carbon dioxide exchange: CarbonTracker, P. Natl. Acad. Sci. USA, 104, 18925–18930, 2007.

Peylin, P., Law, R. M., Gurney, K. R., Chevallier, F., Jacobson, A. R., Maki, T., Niwa, Y., Patra, P. K., Peters, W., Rayner, P. J., Rödenbeck, C., van der Laan-Luijkx, I. T., and Zhang, X.: Global atmospheric carbon budget: results from an ensemble of atmospheric CO_2 inversions, Biogeosciences, 10, 6699–6720, doi:10.5194/bg-10-6699-2013, 2013.

Poulter, B., Cadule, P., Cheiney, A., Ciais, P., Hodson, E., Peylin, P., Plummer, S., Spessa, A., Saatchi, S., Yue, C., and Zimmermann, N. E.: Sensitivity of global terrestrial carbon cycle dynamics to variability in satellite-observed burned area, Global Biogeochem. Cy., 29, 207–222, doi:10.1002/2013GB004655, 2015.

Prentice, C., Heimann, M., and Sitch, S.: The Carbon Balance of the Terrestrial Biosphere: Ecosystem Models and Atmospheric Observations, Ecol. Appl., 10, 1553–1573, 2000.

Prentice, I. C., Farquhar, G. D., Fasham, M. J. R., Goulden, M. L., Heimann, M., Jaramillo, V. J., Kheshgi, H. S., Le Quere, C., Scholes, R. J., and Wallace, D. W. R.: The carbon cycle and atmospheric carbon dioxide, in Climate Change 2001: The Scientific Basis, edited by: Houghton, J. T., Ding, Y., Griggs, D. J., Noguer, M., van der Linden, P. J., Dai, X., Maskell, K., and Johnson, C. A., Cambridge University Press, 183–237, 2001.

Rafique, R., Zhao, F., de Jong, R., Zeng, N., and Asrar, G.: Global and Regional Variability and Change in Terrestrial Ecosystems Net Primary Production and NDVI: A Model-Data Comparison, Remote Sens., 8, 177, doi:10.3390/rs8030177, 2016.

Randerson, J. T., Thompson, M. V., Conway, T. J., Fung, I. Y., and Field, C. B.: The contribution of terrestrial sources and sinks to trends in the seasonal cycle of atmospheric carbon dioxide, Global Biogeochem. Cy., 11, 535–560, doi:10.1029/97gb02268, 1997.

Randerson, J. T., Field, C. B., Fung, I. Y., and Tans, P. P.: Increases in early season ecosystem uptake explain recent changes in the seasonal cycle of atmospheric CO_2 at high northern latitudes, Geophys. Res. Lett., 26, 2765–2768, doi:10.1029/1999GL900500, 1999.

Reich, P. B. and Hobbie, S. E.: Decade-long soil nitrogen constraint on the CO_2 fertilization of plant biomass, Nature Climate Change, 3, 278–282, doi:10.1038/nclimate1694, 2013.

Rödenbeck, C., Houweling, S., Gloor, M., and Heimann, M.: CO_2 flux history 1982–2001 inferred from atmospheric data using a global inversion of atmospheric transport, Atmos. Chem. Phys., 3, 1919–1964, doi:10.5194/acp-3-1919-2003, 2003.

Sarmiento, J. L., Gloor, M., Gruber, N., Beaulieu, C., Jacobson, A. R., Mikaloff Fletcher, S. E., Pacala, S., and Rodgers, K.: Trends and regional distributions of land and ocean carbon sinks, Biogeosciences, 7, 2351–2367, doi:10.5194/bg-7-2351-2010, 2010.

Schneising, O., Reuter, M., Buchwitz, M., Heymann, J., Bovensmann, H., and Burrows, J. P.: Terrestrial carbon sink observed from space: variation of growth rates and seasonal cycle amplitudes in response to interannual surface temperature variability, Atmos. Chem. Phys., 14, 133–141, doi:10.5194/acp-14-133-2014, 2014.

Sillen, W. M. A. and Dieleman, W. I. J.: Effects of elevated CO_2 and N fertilization on plant and soil carbon pools of managed grasslands: a meta-analysis, Biogeosciences, 9, 2247–2258, doi:10.5194/bg-9-2247-2012, 2012.

Sitch, S., Smith, B., Prentice, I. C., Arneth, A., Bondeau, A., and Cramer, W.: Evaluation of ecosystem dynamics, plant geography and terrestrial carbon cycling in the LPJ dynamic global vegetation model, Glob. Change Biol., 9, 161–185, 2003.

Sitch, S., Friedlingstein, P., Gruber, N., Jones, S. D., Murray-Tortarolo, G., Ahlström, A., Doney, S. C., Graven, H., Heinze, C., Huntingford, C., Levis, S., Levy, P. E., Lomas, M., Poulter, B., Viovy, N., Zaehle, S., Zeng, N., Arneth, A., Bonan, G., Bopp, L., Canadell, J. G., Chevallier, F., Ciais, P., Ellis, R., Gloor, M., Peylin, P., Piao, S. L., Le Quéré, C., Smith, B., Zhu, Z., and Myneni, R.: Recent trends and drivers of regional sources and sinks of carbon dioxide, Biogeosciences, 12, 653–679, doi:10.5194/bg-12-653-2015, 2015.

Stocker, B. D., Spahni, R., and Joos, F.: DYPTOP: a cost-efficient TOPMODEL implementation to simulate sub-grid spatio-temporal dynamics of global wetlands and peatlands, Geosci. Model Dev., 7, 3089–3110, doi:10.5194/gmd-7-3089-2014, 2014.

Thompson, R.: The relationship of the phase and amplitude of the annual cycle of CO_2 to phenological events, Plant Ecol. Divers., 4, 213–226, doi:10.1080/17550874.2011.615347, 2011.

Thoning, K. W., Tans, P. P., and Komhyr, W. D.: Atmospheric carbon dioxide at Mauna Loa Observatory: 2. Analysis of the NOAA GMCC data, 1974–1985, J. Geophys. Res., 94, 8549, doi:10.1029/JD094iD06p08549, 1989.

Wei, Y., Liu, S., Huntzinger, D. N., Michalak, A. M., Viovy, N., Post, W. M., Schwalm, C. R., Schaefer, K., Jacobson, A. R., Lu, C., Tian, H., Ricciuto, D. M., Cook, R. B., Mao, J., and Shi, X.: The North American Carbon Program Multi-scale Synthesis and Terrestrial Model Intercomparison Project – Part 2: Environmental driver data, Geosci. Model Dev., 7, 2875–2893, doi:10.5194/gmd-7-2875-2014, 2014.

Yang, Z., Washenfelder, R. A., Keppel-Aleks, G., Krakauer, N. Y., Randerson, J. T., Tans, P. P., Sweeney, C., and Wennberg, P. O.: New constraints on Northern Hemisphere growing season net flux, Geophys. Res. Lett., 34, L12807, doi:10.1029/2007GL029742, 2007.

Zaehle, S. and Friend, A. D.: Carbon and nitrogen cycle dynamics in the O-CN land surface model: 1. Model description, site-scale evaluation, and sensitivity to parameter estimates, Global Biogeochem. Cy., 24, 1–13, doi:10.1029/2009GB003521, 2010.

Zaehle, S., Ciais, P., Friend, A. D., and Prieur, V.: Carbon benefits of anthropogenic reactive nitrogen offset by nitrous oxide emissions, Nat. Geosci., 4, 601–605, doi:10.1038/ngeo1207, 2011.

Zeng, N., Qian, H., Roedenbeck, C., and Heimann, M.: Impact of 1998–2002 midlatitude drought and warming on terrestrial ecosystem and the global carbon cycle, Geophys. Res. Lett., 32, L22709, doi:10.1029/2005GL024607, 2005a.

Zeng, N., Mariotti, A., and Wetzel, P.: Terrestrial mechanisms of interannual CO$_2$ variability, Global Biogeochem. Cy., 19, Gb1016, doi:10.1029/2004GB002273, 2005b.

Zeng, N., Zhao, F., Collatz, G. J., Kalnay, E., Salawitch, R. J., West, T. O., and Guanter, L.: Agricultural Green Revolution as a driver of increasing atmospheric CO$_2$ seasonal amplitude, Nature, 515, 394–397, doi:10.1038/nature13893, 2014.

Zhao, F. and Zeng, N.: Continued increase in atmospheric CO$_2$ seasonal amplitude in the 21st century projected by the CMIP5 Earth system models, Earth Syst. Dynam., 5, 423–439, doi:10.5194/esd-5-423-2014, 2014.